Binder-Free Printed PEDOT Wearable Sensors on Everyday Fabrics Using Oxidative Chemical Vapor Deposition

Michael Clevenger^{1,#}, Hyeonghun Kim^{1,#}, Han Wook Song², Kwangsoo No³, Sunghwan Lee^{1*}

These authors contributed equally to this work.

Keywords: PEDOT, CVD polymer, breathable sensor, binder free, healthcare monitoring

¹ School of Engineering Technology, Purdue University, West Lafayette, IN 47907, USA

² Center for Mass and Related Quantities, Korea Research Institute of Standard and Science, Daejeon 34113, South Korea

³ Department of Materials Science and Engineering, KAIST, Daejeon 34141, South Korea

^{*} Corresponding authors: sunghlee@purdue.edu

Abstract

Polymeric sensors on breathable and flexible fabrics have vast potential towards the development of versatile applications, particularly when the ready-made wearable or fabric can be directly coated. However, traditional coating approaches, such as solution-based methods, have limitations in achieving uniform and thin films due to the poor surface-wettability of fabrics. Herein, to realize a uniform poly(3,4 ethylenedioxythiophene) (PEDOT) layer on various everyday fabrics, we utilize oxidative chemical-vapor-deposition (oCVD). The oCVD technique is a unique method capable of forming patterned polymer films with controllable thicknesses while maintaining the inherent advantages of fabrics, such as exceptional mechanical stability and breathability. Based on the superior characteristics of oCVD PEDOT, we succeed in fabricating blood pressure and respiratory rate monitoring sensors by directly depositing and patterning PEDOT on commercially available disposable gloves and masks, respectively. Those results are expected to pave efficient and facile ways for skin-compatible and affordable sensors for personal healthcare monitoring.

Introduction

With the upsurge of interest in health monitoring systems and non-invasive human/machine interfaces, wearable and stretchable electronic devices have been extensively studied in the past decade (1-6). In particular, wearable sensors that are capable of extracting important bio-information such as body temperature (5), blood pressure (3), or respiratory patterns (6) from the human body without the aid of medical experts and immobile instruments have demonstrated particular promise for the development of future portable health care systems. While the development of these sensory devices are specifically tailored and specialized depending on which types of bio information are being analyzed, or where the intended location of the sensor is being placed, the flexibility and robustness of these sensors must be ensured to guarantee the compatibility of the device on any location of the human body and the prolonged service despite undergoing the mechanical stress and strain caused by daily motion (1-6).

In an effort to provide flexibility, elastomers such as polyimide, polydimethylsiloxane, or fabrics have been adopted as device substrates (1-6). Among them, fabrics have shown tremendous advantages in remarkable stability, skin compatibility, breathability, and in being lightweight (7-9). Moreover, if a sensor is able to be directly fabricated onto ready-made wearables, such as clothes, gloves, or disposable masks, one can monitor their health status with minimized inconvenience. However, owing to the rough nature of the fabric surface, high porosity, and surface hydrophobicity, the formation of a uniform sensing film on the fabric has been regarded as a daunting task compared to developing films on flat and rigid substrates. This issue is especially noticed when using solution-processed conductive polymers, which are one of the most commonly utilized materials for wearable sensors, because the thin-film formation of the materials relies on a liquid-phase deposition technique and its processing requirements such as surface wetting.

Solution-based techniques, such as in situ chemical polymerization (10-12), dip-coating (13-16), or drop-casting methods (17, 18) have been utilized for coating a polymeric film onto a fabric. However, these conventional methods have been limited due to the requirements of suitable surface-wettability and required chemical functional groups on the fabrics for binding liquid-phase monomers or dispersed polymers in a solvent. In addition, the harsh conditions required for the liquid-based methods, such as necessary acid-treatment or annealing processing temperatures higher than 150 °C (14, 19), have become another factor limiting the types of candidates for sensor substrates. Furthermore, the usage of additives, such as binders, that are often used for improving conformability of versatile fabrics, ultimately failed to maintain the inherent advantages of the fabrics (e.g., breathability or skin compatibility), as well as ultimately lower the conductivity due to the insulating nature of the binder (20-22).

Oxidative chemical vapor deposition (oCVD) has recently emerged as an innovative and unique method for synthesizing conductive polymer films with superior conductivity (23-25). Functionally, the conductive polymer films are synthesized through the polymerization of a vaporized monomer and oxidizing agent. The vapor-phase reagents uniformly coat the whole surface of any substance regardless of surface morphology and wetting properties, enabling highly uniform polymer layers on virtually any substrates. The outstanding step-coverage facilitated by the oCVD technique has been a breakthrough for a wide range of research fields such as lightemitting diodes (26), lithium-ion batteries (27), or redox-flow batteries (28), where oCVD polymers have been conformally coated on vertically aligned nanowires or porous media. However, for wearable sensors, there has been limited progress to date.

Herein, we utilize the oCVD technique for creating a conformal poly(3,4-ethylene dioxythiophene) (PEDOT) layer on multiple fabrics (nylon, polyester, and cotton) and disposable

wearables (commercially available glove and mask) for sensory devices without any binders or additives. The oCVD technique is capable of creating a highly conductive PEDOT film where thickness is readily controllable from ~10 nm to thicker than 1 μm by varying the deposition time. Moreover, the mechanical stability, breathability, and lightness of fabrics are consistent even after the PEDOT coating, implying oCVD PEDOT is notably promising as an active material for potential wearable devices. Based on the unique properties associated with oCVD deposited PEDOT, we fabricate prototype resistive sensors by directly printing PEDOT on a commercially available disposable glove and mask, made of polymer fabrics such as polypropylene or polyester. The sensors successfully demonstrate capabilities of extracting blood pressure information and respiratory rates in real-time with remarkable precision. This is the first report proving the usability of the oCVD method on fabric-based sensors, thus, paving the way for developing versatile healthcare devices.

Results

Schematic of oCVD and characterization of oCVD PEDOT deposited on fabrics

The oCVD technique offers clear advantages over solution-based polymer coating methods due to its ability to conformally coat complex geometries regardless of surface functionalities (e.g., hydrophobicity). Shown in Fig. 1A, a schematic of the oCVD chamber illustrates the gas-phase deposition process. EDOT monomers are vaporized and metered into the chamber via a needle valve, in which the monomers react with sublimated FeCl₃ (oxidizing agent). The structure of the oCVD reactors is further described in Fig S1. Through step-growth polymerization, PEDOT chains are deposited onto the upside-down substrate. The substrates can be mounted in a way in which shadow-masking is possible to selectively exposed areas. An example of this can be viewed

in Fig. 1B, where a Purdue "P" was patterned onto polyester fabric via oCVD deposition of PEDOT, as well as line-patterns onto medical gauze.

Fig. 1C shows Fourier-transform infrared (FTIR) spectra. Comparison between PEDOT films deposited on fabric as well as Si substrates shows clear similarities of peak locations, indicating oCVD PEDOT was well synthesized on fabric. The peak located at a wavelength of ~1550 nm is related to C=C stretching indicative of standard PEDOT films in the thiophene ring and is observed in PEDOT on both fabric and Si substrates. Peak presence at ~1425 nm on both fabric and Si substrates indicates both C-C and C-H bonds, characteristic of PEDOT films. The additional presence of the C-O bond located at ~1350 nm is shared between the films deposited on both substrates. Strong peaks shown at ~1080, 1110, and 1160 nm represent prominent C-O-C bonding, indictive of the ethylenedioxy group. In short, FTIR spectra of oCVD PEDOT films identified the characteristic chemical bonds of C=C, C-C, C-H, S, and C-O-C, which are coincided with previous works, solidifying the claim of successful PEDOT deposition on a fabric substrate (29, 30).

In order to confirm the mechanical flexibility of PEDOT films, bending tests were conducted on fabric samples coated with various thickness oCVD PEDOT films deposited at different substrate temperatures. For the bending test, the samples were bent 180° to generate high stress and strain on the fabrics and their sheet resistances were measured every cycle. Values of sheet resistance (R_s) were then converted to the comparable term conductivity, which is regarded as nominal compared to standard conductivity measurements on flat surfaces, using the equation, $\sigma=1/(R_s \times t)$ with the film thickness, t. PEDOT deposited on fabric was shown to maintain its conductive performance more than 100 bending cycles (Fig. 1D). This exemplifies

PEDOT's excellent mechanical flexibility, resilience to bending and strain cycles that typical wearable fabrics would undergo.

Comparing PEDOT films (~200 nm-thick) deposited at various temperatures, the conductivity of PEDOT notably increases with higher substrate temperatures. To investigate the temperature effect in more detail, we investigated the conductivity of PEDOT, grown on flat glass substrates at various deposition temperatures from 50-130 °C. From this investigation, Fig. S2 demonstrates the conductivity increases linearly below 100 °C. FTIR (Fig. S3) and AFM (Fig. S4) analysis of the films substantiate that high deposition temperatures lead to a longer conjugation length and larger grain-like structures of oCVD PEDOT films, both of which are eligible factors to increase the conductivity of the polymer (*30, 48-49*). Moreover, the uniform coverage of the oCVD PEDOT on fabrics could be achieved even as the thickness of the polymer is up to 1 μm (Fig. S5).

A breathability test was conducted to determine whether the air permeability of the fabrics is compromised due to the coated PEDOT film on the fabric. The test consisted of covering and sealing vials filled with DI water with bare fabric or oCVD PEDOT-deposited fabric of varying thicknesses. The vials were then heated via a hotplate in order to encourage water evaporation. The resulting water vapor would then permeate through the fabrics into the surrounding environment. In order to track the amount of water released, the mass of the water was measured at specific intervals across 48 hours. The relationship of remaining water mass in the vials to time can be shown in Fig. 1E. From the figure, the rate of evaporation for bare fabric can be found to be ~0.036 g hr⁻¹. oCVD PEDOT's rate was found to be ~0.031 g hr⁻¹, showing a negligible change in breathability from bare fabric to oCVD PEDOT deposited fabric. Amongst oCVD PEDOT fabrics, no clear difference is seen between fabrics of varying thicknesses, showcasing oCVD

PEDOT's ability to maintain fabric breathability regardless of film thickness. This consistent high breathability indicates the enhanced versatility of oCVD PEDOT for wearable devices as film thickness can be adjusted per application without having to consider the effect on breathability.

Comparison between oCVD PEDOT and solution-processed PEDOT:PSS

In order to visualize the clear benefits of the oCVD deposition technique over traditional solution-based processing, oCVD PEDOT and solution-processed PEDOT:PSS (deposited via dip-coating) were applied on three different fabric types: nylon, polyester, and cotton. We selected a standard PEDOT:PSS solution as a representative material for a solution process, considering its same polymer backbone structure as oCVD PEDOT. As shown in Fig. 2A, the oCVD process succeeded in coating uniform films on all the fabrics. However, the dip-casting process failed at uniform coating on hydrophobic fabrics like nylon and polyester. While there is a slight increase in wettability for PEDOT:PSS deposited on cotton fabrics, the resulting films are still highly non-uniform as evidenced by the uneven coloration indicating thickness variation across the film.

Simple rectangular channels were created on fabric utilizing both oCVD PEDOT and PEDOT:PSS in order to compare the spatial uniformity between the oCVD PEDOT and solution-based PEDOT:PSS films (Detail method is described in Supplementary Materials with Fig. S6). In this case, channel length was varied between 6-30 mm while channel width was kept constant. As shown in Fig. 2B, oCVD PEDOT clearly follows standard channel-length modulation practices, as the resistance scales linearly with channel length with minimal error amongst multiple samples. However, PEDOT:PSS fabric showed a much larger variation in resistance as well as the lack of a linear trend with the channel length, indicating that the solution-based coating does not yield uniform conductance of the film grown on fabric, compared to the oCVD PEDOT. It is expected that any polymer solutions are difficult to be uniformly coated on various substrates due to the

material-dependent wettability issues. In contrast, the vapor-phase oCVD process is capable of uniform polymer coating virtually on any type of substrates including fabric, thus has greater benefits for fabricating fabric-based devices.

Scanning electron microscopy (SEM) images of oCVD PEDOT and PEDOT:PSS deposited onto polyester fabrics are shown before and after bending in Fig. 2C. SEM images were taken to confirm the conformality of oCVD PEDOT films on fabric threads vs. the non-uniformity consistently observed in PEDOT:PSS throughout this study. The threads in PEDOT:PSS films are significantly bridged by the PEDOT:PSS coating, reducing the open pore ratio of fabric and critically limiting the breathability. oCVD PEDOT, on the other hand, shows clear conformality, both before and after 100 bending cycles. PEDOT:PSS, however, shows significant film tearing and separation from threads after bending, leading to overall lack of uniformity and performance of PEDOT:PSS when compared to oCVD PEDOT. The notable uniformity difference between oCVD PEDOT and PEDOT:PSS could be also identified for nylon and cotton fabrics as shown in Fig. S6.

To confirm the mechanical flexibility of oCVD PEDOT, bending tests were conducted to examine the change in overall resistance, and therefore conductivity of oCVD PEDOT films throughout bending. The results were compared to those of traditional solution-processed PEDOT:PSS. From the plot in Fig. 2C, it can be seen that throughout bending oCVD PEDOT maintains its nearly identical resistance level, and therefore conductivity with only a 4% deviation across all cycles from its initial measurement. PEDOT:PSS, however, showed a 400% increase in resistance, indicating significant amounts of degradation. The occurrence of this degradation can be clearly explained by the tendency for PEDOT:PSS films to tear and separate, as shown in Fig. 2D. The mechanical flexibility and reliable conductivity performance of oCVD PEDOT, despite

undergoing multiple bending cycles, highlights the efficacy of the oCVD vapor-phase deposition technique and its ability to conformally coat complex geometries with high film uniformity.

Wearable sensors using oCVD PEDOT

The oCVD PEDOT having demonstrated exceptional conformability on fabrics and stability has much potential to be implemented as an active material for sensor applications. Herein, we fabricated prototype wearable sensors by directly depositing oCVD PEDOT onto commercially available disposable gloves and masks. Fig. 3A demonstrates a schematic and a photograph (inset) for a pressure sensor printed on a glove of which thread consists of a mixture of polyester and polyethylene. The tip of the index finger was covered by patterned oCVD PEDOT of 1.5 cm of length and 0.5 cm of width. The ends of the PEDOT were then connected with copper electrode tape connected to a source meter.

The current change, recorded at a bias of 0.1 V, was investigated under a wide range of pressures (Figs. 3B-E). The sensitivity tests were conducted by pressing the PEDOT film with a weight-loaded slide glass. The current dramatically increased by 1,400% when 1.8 kPa of pressure is applied to the center of the PEDOT film (Fig. 3B). Even when undergoing a minute pressure of 200 Pa (the inset of Fig. 3B), a significant response was still observable (200% change). The current drops, occurring from the moment of pressing and releasing, were attributed to transitory charge generation caused by the triboelectric effect between the glass and the PEDOT surface (Fig. S8). In general, the triboelectric phenomenon takes place in a short moment (< 10 ms) and rapidly reaches an equilibrium state. Therefore, as shown in Fig. S8, the sensing response (current variation, recorded at the equilibrium state) was not significantly disturbed by the triboelectric effect. The sensitivity is defined as $\delta(\Delta I/I_0) / \delta P$, where I_0 is the initial current, and ΔI is the current change (%) induced by applying pressure (P). The oCVD PEDOT sensor demonstrated a notable

sensitivity of 8 kPa⁻¹, which is enough to use the oCVD-based fabric sensor for the measurement of various bioinformation from the human body (Fig. 3C). As a significant figure of merit for pressure sensors, we also measured the operation rates of the PEDOT sensor. The response time is defined as the time period required for the current level to reach 90% of the saturation state as pressure is applied, while the recovery time is the time period to reach 10% of the saturation level after the pressure is removed (Fig. 3D). Response and recovery times of 260 and 30 ms, respectively, were recorded while applying and releasing an approximate pressure of 1.8 kPa. It should be noted that the performance of oCVD PEDOT sensors is comparable to previously reported resistive devices based on conductive polymers (Table S1) (31-44), even without any additives or sophisticated device structure in our sensors.

The working principle of the oCVD PEDOT sensor is described in Fig. 3F. As with other typical fabrics, the glove consists of "warp" and "weft" threads, one of which wraps the other in the vertical direction. When the oCVD process is initiated, the gas-phase monomers and oxidizing agents cover every open-facet of the yarn, and the PEDOT layer uniformly coats the exposed surfaces. In contrast, the adhered region between warp and weft (denoted as the shaded region), which is too compact to permit the access of the gas molecules, is not coated by the conductive PEDOT film and still remains a non-conductive region. With no pressure applied, the selective surface covering makes the current flow in the fabric only through the internal path on each thread. When pressure is applied, the flexible PEDOT coated threads are structurally deformed as shown in the right of Fig. 3F. Compared to the unpressured state, the deformation increases the contact area of the PEDOT films between the warp and weft, which creates an additional current path. In this case, the current flows not only through a single thread but also through multi-conductive paths from the cross-over between threads. This is the operational mechanism of the oCVD

PEDOT-based fabric sensor where the overall conductivity is proportional to the applied pressure (Fig. 3C). Moreover, the elasticity of polymers is high enough to restore the cross-over state to an unpressured state rapidly once the pressure is removed, enabling the fast recovery behavior as shown in Fig. 3E.

Based on the high sensitivity and fast response rates, the oCVD PEDOT sensor was expected to qualify for tracking blood pressure information. The pressure range (< 2 kPa), used for investigating the sensitivity of our sensor, is much lower compared to an actual blood pressure (BP) which is in a range of 10-16 kPa (80-120 mmHg). However, the pivotal goal of the glove sensor in this research is to identify a BP pattern measuring the associated pressure changes from a pulse at the wrist or neck under a mild pressing condition. Using this mild pressure condition, a user is equipped with the device with minimal inconvenience, unlike conventional cuff-type BP instruments that compress an arm or wrist until blood flow is blocked. Pang et al. utilized an ultralight strain-gauge sensor and fixed it gently on a wrist to monitor a BP pattern (51). They succeeded in tracking the pattern information in real-time with minimized discomfort even though the recorded pressure value was in a range of 500 Pa, much less than that of the actual BP. Likewise, we targeted to measure BP patterns under a similarly mild pressing condition, for which we chose the polyethylene fabric due to its readily deformative characteristic under low pressures.

Fig. 3G demonstrates regular pulse patterns, which were measured by placing the fabric sensor onto the radial artery located in the wrist. The radial artery pulse consists of two significant components (Fig. 3H); one (P1) is caused by the main blood pressure from the first beat of the pulse, and the other (P2) represents the reflected peak wave from the secondary beat. The radial artery augmentation index (AI), defined as a ratio of the peak intensities (P1/P2), has been studied as an indicative sign for diagnosing cardiovascular diseases. The AI estimated from the oCVD

PEDOT sensor was 0.55, within the normal range of a healthy 20-30 year-old individual (45-47). In addition, the oCVD PEDOT sensor succeeded in extracting the blood pressure patterns from the neck to measure carotid artery pressure. The carotid AI value (0.38) was slightly lower than that of radial artery pulse and consistent with reported clinical trials (47). Those results substantiate the capability of the glove sensor to extract meaningful blood pressure information from multiple points in the human body without the aid of medical experts and immobile instruments. To test the stability and endurance of our sensors, we submitted PEDOT coated fabrics to repeated standard use tests and abrasion cycles. The standard use test consisted of applying our sensor to the skin in concurrence with the typical use outlined for the BP sensor. For the abrasion cycles, the surface of the PEDOT film was repeatedly rubbed against the skin to examine the potential of wear. Each of these tests was conducted across 200 cycles, where the current change was recorded after pressure removal at a voltage of 0.1V. The results, which can be viewed in Fig. S9, showed no degradation of base current after undergoing all 200 cycles of abrasion and standard use, showcasing the endurance capabilities of our sensors.

Respiratory rate is a significant physiological indicator capable of diagnosing severe respiratory diseases such as cardiopulmonary arrest, chronic heart failure, or pneumonia. In particular, with a dramatic surge of COVID-19, handy and affordable sensors equipped with disposable masks have been extensively demanded. In this regard, we fabricated the oCVD PEDOT sensor on a conventional, commercially available, disposable mask, consisting of two non-woven fabrics (a mixture of Spandex and polypropylene) and a melt blown filter (polypropylene) interposed between them (Fig. 4A). It should be noted that the oCVD technique provides an exceptional capability to form a uniform and thin patterned PEDOT film (~100 nm) on the mask directly without any secondary assembling processes.

Fig. 4B compares current change, recorded at a bias of 0.1 V, before and after 5 min exercise (running). The signal of the mask sensor is susceptible to environmental conditions and the facial shape of the subject. Besides the base current is expected to gradually shift during longterm use. Therefore, for the practical use of the sensor, the current fluctuation, affected by the exterior reasons, should be corrected based on a proper signal processing algorithm to extract respiratory information automatically. The procedure for the data processing is described in the Supplementary Materials with Fig. S11 in more detail. The initial rate was 16-20 min⁻¹, which is raised up to 40-42 min⁻¹ after running. The pattern was completely restored after enough rest time (>10 min). A single breath pulse for each state is described in Figs. 4C and 4D. For both normal and running states, inhalation caused a current drop which is recovered during exhalation. The period was shortened from 3.0-3.8 s to 1.4-1.5 s after exercise, and the amount of current change for each cycle was far beyond the noise level of our sensor, ensuring a precise measurement. With the standard respiratory rate for an adult being between 12-20 min⁻¹, and the abnormal rate being either below 12 min⁻¹ or above 25 min⁻¹ (52-55), by showcasing the clear change in rate from 16-20 min⁻¹ to 40-42 min⁻¹ after running, and then a decrease back to 12-14 min⁻¹, the mask sensor has shown the capability to measure the respiration rate and to detect the difference between normal and abnormal ranges, which is an important factor in identifying potential illnesses associated with abnormal respiratory rate including, but not limited to, lung degradation, anxiety, fever, and cardiac conditions (52-55).

To identify the working principle of the mask sensor in more detail, we conducted additional electrical measurements (Fig. S10) which emulates the working environment of the mask sensor. For a case where the sensor is placed on a compact glass slide and its two ends fixated (Fig. S10B), the vertical pressing (1 kPa) on the sensor did not cause a significant current rise (Fig.

S10C), contrary to the glove sensor (Fig. 3). For the glove sensor, which is much more sensitive to applied vertical pressure, the current increment is attributed to the contact resistance variation between the warp and weft threads, accompanied by the structural deformation of those threads. However, the non-woven outer fabric in the mask, which is previously compressed during its manufacturing process, consists of too compactly stacked threads (the inset of Fig. S10A) to be transformed under mild pressure. Thus, the mask sensor was relatively insensitive to the applied vertical pressure.

Instead, if the two ends of the sensor were only attached to glass substrates while the center part was free-standing as shown in Fig. S10D, the pressure applied on the center of the fabric caused the current drop (Fig. S10E) of which the amount of variation was 8.5 times more than that of the first case (Fig. S10B and C). The underlying principle of the current change for the second case is based on the elongation of the fabric induced by the pressure. The electrical resistance of the PEDOT-coated outer non-woven fabric, consisting of compactly stacked threads, is determined by the combination of the internal resistance of each PEDOT-coated thread and the contact resistance between them. During the elongation, some of the conjunction points between threads are disconnected, bringing about a depression of charge transport through the inter-thread path which is related to the contact resistance; thus, the significant current drop that appeared during the pressing.

When the mask is equipped and fixated around the face, an air gap exists around the nostrils and mouth. The softness of fabrics allows shrinkage and recovery of the space accompanied by the instant structural deformation of the mask during repeated respiration. Considering the inhalation process, the air gap is gradually curtailed, and the center of the mask is bent inward (the bottom of Fig. 4A) which is similar to the deformation described in Fig. S10D. As discussed above,

some conjunction points between the PEDOT-coated threads are detached during the elongation caused by the inhalation, resulting in an incremental change of the contact resistance between the PEDOT layers. As exhalation initiates, the deformation and change in conductivity from the induced gap are recovered to that of the normal condition. Thus, a repeatable breathing pattern can be electronically recorded by the real-time measurement of resistance of the PEDOT coated layer.

Discussion

Herein, we explored the conformability of the oCVD method on multiple fabrics (nylon, polyester, and cotton). The vapor-phase injection of reactants enables a uniform coating on any substrate regardless of their porosity or hydrophobicity. The thickness of the coating is controllable from 10 to thicker than 1000 nm by varying deposition time and temperature. Notably, compared to a dipcasting method using the PEDOT:PSS solution, the oCVD PEDOT's bendability was exceptionally superior while maintaining the inherent advantages of fabrics such as breathability. Based on the outstanding features of oCVD PEDOT as an active material for wearable devices, we fabricated two prototype sensors by directly patterning and depositing PEDOT on a commercially available disposable glove and mask. The glove sensor successfully served as a precise pressure sensor, capable of extracting blood pressure information from the radial or carotid artery by simply touching the wrist or neck. The respiratory rate monitoring sensor, printed on the disposable mask, was able to monitor breathing patterns in real-time. To the best of our knowledge, this is the first report of vapor-printing sensors directly fabricated on ready-made masks. The utilization of the oCVD technique, paired with the conjugated polymer PEDOT has proven to be certainly advantageous in terms of strong adhesion between the sensing layer and wearable fabrics, contrary to conventional approaches of which the sensory parts need to be prepared separately first, and then assembled later on the resulting wearable. Therefore, the oCVD process is a groundbreaking addition towards the development of wearable devices in ready-made clothes (or masks) that can monitor personal healthcare information without the aid of medical experts and immobile instruments.

While the scope of our paper was the development of low-cost disposable sensors, which were intended to limit any potential spread of contagious diseases and therefore did not require a washing capability, the challenge of longevity is definitely of great consideration. Since the majority of polymers are typically not known for their resistance to large amounts of direct water and detergent contact like general electrical components, the initial focus of this research was made on manufacturing one-time sensors. However, we are considering potential methods to mitigate this challenge through the examination of gas-phase passivation, film thickness modulation, or composite film generation compatible with the oCVD process utilizing additional substances better suited for increased longevity when facing washing cycles. We believe that the progress would broaden the application of the CVD polymer technique into versatile wearable electronic applications.

Materials and Methods

oCVD process, oCVD PEDOT thin films were deposited on glass, silicon (Si), and fabric substrates using a custom reactor (Fig. S1) which is an enclosed sealed chamber that maintains conditions to allow for vapor phase polymerization. 3,4-Ethylenedioxythiophene (EDOT, 97%, Sigma Aldrich) monomer vapors were metered into the chamber using a needle valve after being heated to 130 °C to vaporize. Iron chloride oxidizing agent (FeCl₃, reagent grade, Sigma Aldrich), stored in a crucible in the main chamber, is sublimated by heating the crucible to 180 °C at a ramping rate of approximately 10 °C per minute. The working pressure was maintained as 2×10^{-3} torr through the adjustment of the flow rate of the needle valve. Once both the vaporized monomer and oxidizing agent were introduced and a consistent chamber pressure was achieved, the deposition was initiated by opening the main shutter which covers the substrate. The substrate was maintained at a constant specified temperature (30-100 °C), dependent on the sample, and the thickness was controlled by varying the deposition time. Finally, the PEDOT-coated samples were rinsed with methanol (J. T. Baker) for 10 min to remove un-reacted FeCl₃ and EDOT monomers and dried in a vacuum desiccator to evaporate the methanol solvent completely. Once completely dried, PEDOT-coated silicon samples were measured for thickness utilizing a FilmSense FS-1 Ellipsometer. This thickness measurement was used as the nominal thickness for all PEDOTcoated fabric samples deposited concomitantly with the silicon samples (56, 57). Comparing the nominal thickness with the cross-sectional SEM images, directly obtained from PEDOT-coated nylon samples (Fig. S12), revealed less than a 5% difference in thickness and therefore clearly validated the indirect thickness monitoring approach used in this study.

PEDOT:PSS coating on fabrics. Fabrics, pre-cleaned by IPA, were dip-casted into a PEDOT:PSS solution (PH 1000, Ossila) for 30 min to adsorb the required amount of polymers. The samples were then annealed on a 50 °C hot plate for 30 min and stored in a vacuum desiccator for a day to eliminate the residual solvents.

Materials characterization. Functional groups on PEDOTs were analyzed utilizing Fourier-Transform Infrared Spectroscopy (FTIR, Nexus 670 ThermoNicolet Spectrometer) with an Attenuated Total Reflection (ATR) accessory. PEDOT films on fabrics were observed using Thermo Fischer Scientific Teneo scanning electron microscope (SEM). The breathability test consisted of filling vials with 3 ml of deionized water. The fabric samples were then placed over

the top opening of the vials and sealed around the edge through rubber banding. Vials were then placed equidistant from each other on a hot plate heated to 120 °C. Breathability was then calculated via the change in total mass from the evaporation of the water across the test.

Sensor fabrication and characterization. After deposition of PEDOT on fabrics (disposable glove and mask) with a pre-patterned shadow mask, two separated copper electrode tabs were bonded on the conductive polymer. Silver paste and carbon tape were interposed between the copper and polymer films to fix them more tightly and minimize electrical noise. The sensor measurements were conducted using a source meter (Agilent 4155B). Alligator clips were used to connected the sensor with the source meter, and the measurement was implemented at a bias of 0.1 V.

Supplementary Materials

Section S1 Methods

Table S1 Comparison of the performances of conductive polymer-based pressure sensors.

Figure S1 An overall schematic of the oCVD reactor.

Figure S2 Conductivity of oCVD PEDOT depending on deposition temperature.

Figure S3 FTIR spectra of oCVD PEDOT depending on deposition temperature.

Figure S4 AFM images of oCVD PEDOT depending on deposition temperature.

Figure S5 SEM images of bare and PEDOT-coated fabrics with different polymer thicknesses.

Figure S6 A photo image of Ag paste electrodes, captured after PI tape masks removed.

Figure S7 SEM images of oCVD PEDOT and PEDOT:PSS coated fabrics.

Figure S8 A transient current change of the sensor, protected with and without a protection PE layer, under applying a pressure of 200 Pa.

Figure S9 Sustainability tests.

Figure S10 Investigation of the working principle of the oCVD PEDOT-based mask sensor.

Figure S11 Signal processing for the mask sensor.

Figure S12 Thickness of the oCVD PEDOT directly measured from PEDOT-coated fabric.

Acknowledgments

Funding: This work was partially supported by the U.S. National Science Foundation (NSF) Award No. ECCS-1931088. S.L. and H.W.S. acknowledge the support from the Improvement of Measurement Standards and Technology for Mechanical Metrology (Grant No. 20011028) by KRISS. K.N. was supported by Basic Science Research Program (NRF-2021R11A1A01051246) through the NRF Korea funded by the Ministry of Education.

Competing Interests

The authors declare that they have no competing interests.

Author Contributions

S.L., M.C. and H. K. conceived the study. M.C. prepared the materials. H.K. fabricated the devices. M.C. and H.K. performed the measurements. M.C., H.K., H.W.S and K.N. analyzed the data. M.C., H.K., and S.L. wrote the manuscript, with input from H.W.S and K.N.

Data and materials availability

All data needed to evaluate the conclusions in the paper are present in the paper and/or the Supplementary Materials.

References and Notes

- 1. C. Wang, K. Xia, H. Wang, X. Liang, Z. Yin, Y. Zhang, Advanced carbon for flexible and wearable Electronics. *Adv. Mater.* **31**, 1801072 (2019).
- 2. M. Amjadi, K.-U. Kyung, I. Park, M. Sitti, Stretchable, skin-mountable, and wearable strain sensors and their potential applications: A review. *Adv. Funct. Mater.* **26**, 1678-1698 (2016).
- 3. Y. Liu, M. Pharr, G. A. Salvatore, Lab-on-skin: A review of Flexible and stretchable electronics for wearable health monitoring. *ACS Nano* **11**, 9614-9635 (2017).
- 4. A. Nag, S. C. Mukhopadhyay, Wearable flexible sensors: A review. *IEEE Sens. J.* **7**, 3949-3960 (2017).
- 5. Q. Li, L.-N. Zhang, X-.M. Tao, X. Ding, Review of flexible temperature sensing networks for wearable physiological monitoring. *Adv. Healthcare. Mater.* **6**, 1601371 (2017).
- 6. A. Servati, L. Zou, Z. J. Wang, F. Ko, P. Servati, Novel flexible wearable sensor materials and signal processing for vital sign and human activity monitoring. *Sensors.* **17**, 1622 (2017).
- 7. S. Seyedin, P. Zhang, M. Naebe, S. Qin, J. Chen, X. Wanga, J. M. Razal, Textile strain sensors: A review of the fabrication technologies, performance evaluation and applications. *Mater. Horiz.* **6**, 219-249 (2019).
- 8. J. S. Heo, J. Eom, Y.-H. Kim, S. K. Park, Recent progress of textile-based wearable electronics: A comprehensive review of materials, devices, and applications. *Small.* **14**, 1703034 (2018).
- 9. G. Acar, O. Ozturk, A. J. Golparvar, T. A. Elboshra, K. Böhringer, M. K. Yapici, Wearable and flexible textile electrodes for biopotential signal monitoring: A review. *Electronics*. **8**, 479 (2019).
- 10. K. Opwis, D. Knittel, J. S. Gutmann, Oxidative in situ deposition of conductive PEDOT:PTSA on textile substrates and their application as textile heating element. *Synth. Met.* **162**, 1912-1918 (2012).
- 11. A. Hebeish, S. Farag, S.Sharaf, T. I. Shaheen, Advancement in conductive cotton fabrics through in situ polymerization of polypyrrole-nanocellulose composites. *Carbohydr. Polym.* **151**, 96-102 (2012).
- 12. N. D. Tissera, R. N. Wijesena, S. Rathnayake, R. M. de Silva, K. M. N. de Silva, Heterogeneous in situ polymerization of polyaniline (PANI) nanofibers on cotton textiles: Improved electrical conductivity, electrical switching, and tuning properties. *Carbohydr. Polym.* **186**, 35-44 (2018).
- 13. D. Pani, A. Dessì, J. F. Saenz-Cogollo, G. Barabino, B. Fraboni, A. Bonfiglio, Fully textile, PEDOT:PSS based electrodes for wearable ECG monitoring systems. *IEEE Trans. Biomed. Eng.* **63**, 540-548 (2016).
- 14. Y. Ding, M. A. Invernale, G. A. Sotzing, Conductivity trends of PEDOT-PSS impregnated fabric and the effect of conductivity on electrochromic textile. *ACS Appl. Mater. Interfaces.* **2**, 1588-1593 (2010).
- 15. A. Ahmed, M. A. Jalil, M. M. Hossain, M. Moniruzzaman, B. Adak, M. T. Islam, M. S. Parvez, S. Mukhopadhyay, A PEDOT:PSS and graphene-clad smart textile-based wearable

- electronic joule heater with high thermal stability. J. Mater. Chem. C 8, 16204-16215 (2020).
- 16. Y. Ding, J. Yang, C. R. Tolle, Z. Zhu, Flexible and compressible PEDOT:PSS@Melamine conductive sponge prepared *via* one-step dip coating as piezoresistive pressure sensor for human motion detection. *ACS Appl. Mater. Interfaces* **10**, 16077-16086 (2018).
- 17. I. Nuramdhani, M. Jose, P. Samyn, P. Adriaensens, B. Malengier, W. Deferme, G. D. Mey, L. V. Langenhove, Charge-discharge characteristics of textile energy storage devices having different PEDOT:PSS ratios and conductive yarns configuration. *Polymer* 11, 345 (2019).
- 18. I. del Agua, D. Mantione, U. Ismailov, A. Sanchez-Sanchez, N. Aramburu, G. G. Malliaras, D. Mecerreyes, E. Ismailova, DVS-crosslinked PEDOT:PSS free-standing and textile electrodes toward wearable health monitoring. *Adv. Mater. Technol.* **3**, 1700322 (2018).
- 19. H. Shi, C. Liu, Q. Jiang, J. Xu, Effective approaches to improve the electrical conductivity of PEDOT:PSS: A review. *Adv. Electron. Mater.* **1**, 1500017 (2015).
- 20. M. Åkerfeldt, M. Strååt, P. Walkenström, Electrically conductive textile coating with a PEDOT-PSS dispersion and a polyurethane binder. *Text. Res.* J. **83**, 618-627 (2013).
- 21. M. G. Tadesse, D. A. Mengistie, Y. Chen, L. Wang, C. Loghin, V. Nierstrasz, Electrically conductive highly elastic polyamide/lycra fabric treated with PEDOT:PSS and polyurethane. *J. Mater. Sci.* **54**, 9591-9602 (2019).
- 22. J. D. Ryan, D. A. Mengistie, R. Gabrielsson, A. Lund, C. Müller, Machine-washable PEDOT:PSS dyed silk yarns for electronic textiles. *ACS Appl. Mater. Interfaces* **9**, 9045-9050 (**2017**).
- 23. K. K. Gleason, CVD Polymers: Fabrication of Organic Surfaces and Devices (John Wiley & Sons, 2015).
- 24. M. H. Gharahcheshmeh, M. M. Tavakoli, E. F. Gleason, M. T. Robinson, J. Kong, K. K. Gleason, Tuning, optimization, and perovskite solar cell device integration of ultrathin poly(3,4-ethylenedioxythiophene) films *via* a single-step all-dry process. *Sci. Adv.* 5, eaay0414 (2019).
- 25. M. H. Gharahcheshmeh, K. K. Gleason, Device fabrication based on oxidative chemical vapor deposition (oCVD) synthesis of conducting polymers and related conjugated organic materials. *Adv. Mater. Interfaces* **6**, 1801564 (2019).
- 26. L. Krieg, F. Meierhofer, S. Gorny, S. Leis, D. Splith, Z. Zhang, H. von Wenckstern, M. Grundmann, X. Wang, J. Hartmann, C. Margenfeld, I. M. Clavero, A. Avramescu, T. Schimpke, D. Scholz, H.-J. Lugauer, M. Strassburg, J. Jungclaus, S. Bornemann, H. Spende, A. Waag, K. K. Gleason, T. Voss, Toward three-dimensional hybrid inorganic/organic optoelectronics based on GaN/oCVD-PEDOT structures. *Nat. Commun.* 11, 5092 (2020).
- 27. G.-L. Xu, Q. Liu, K. K. S. Lau, Y. Liu, X. Liu, H. Gao, X. Zhou, M. Zhuang, Y. Ren, J. Li, M. Shao, M. Ouyang, F. Pan, Z. Chen, K. Amine, G. Chen, Building ultraconformal protective layers on both secondary and primary particles of layered lithium transition metal oxide cathodes. *Nat. Energy* 4, 484-494 (2019).
- 28. M. H. Gharahcheshmeh, C. T.-C. Wan, Y. A. Gandomi, K. V. Greco, A. Forner-Cuenca, Y.-M. Chiang, F. R. Brushett, K. K. Gleason, Ultrathin conformal oCVD PEDOT coatings

- on carbon electrodes enable improved performance of redox flow batteries. *Adv. Mater. Interfaces* 7, 2000855 (2020).
- 29. S. Lee, K. K. Gleason, Enhanced optical property with tunable band gap of cross-linked PEDOT copolymers *via* oxidative chemical vapor deposition. *Adv. Funct. Mater.* **25**, 85-93 (2015).
- 30. G. Drewelow, H. Wook Song, Z.-T. Jiang, S. Lee, Factors controlling conductivity of PEDOT deposited using oxidative chemical vapor deposition. Appl. Surf. Sci. **501**, 144105 (2020).
- 31. M. Beccatelli, M. Villani, F. Gentile, L. Bruno, D. Seletti, D. M. Nikolaidou, M. Culiolo, A. Zappettini, N. Coppedè, All-polymeric pressure sensors based on PEDOT:PSS-modified polyurethane foam. *ACS Appl. Polym. Mater.* 3, 1563-1572 (2021).
- 32. P. Zhao, R. Zhang, Y. Tong, X. Zhao, T. Zhang, Q. Tang, Y. Liu, Strain-discriminable pressure/proximity sensing of transparent stretchable electronic skin based on PEDOT:PSS/SWCNT electrodes. *ACS Appl. Mater. Interfaces* **12**, 55083-55093 (2020).
- 33. Z. Li, S. Zhang, Y. Chen, H. Ling, L. Zhao, G. Luo, X. Wang, M. C. Hartel, H. Liu, Y. Xue, R. Haghniaz, K. Lee, W. Sun, H. Kim, J. Lee, Y. Zhao, Y. Zhao, S. Emaminejad, S. Ahadian, N. Ashammakhi, M. R. Dokmeci, Z. Jiang, A. Khademhosseini, Gelatin methacryloyl-based tactile sensors for medical wearables. *Adv. Funct. Mater.* 30, 2003601 (2020).
- 34. T. Chen, S.-H. Zhang, Q.-H. Lin, M.-J. Wang, Z. Yang, Y.-L. Zhang, F.-X. Wang, L.-N. Sun, Highly sensitive and wide-detection range pressure sensor constructed on a hierarchical-structured conductive fabric as a human–machine interface. *Nanoscale* 12, 21271-21279 (2020).
- 35. J. J. Lee, S. Gandla, B. Lim, S. Kang, S. Kim, S. Lee, S. Kim, Alcohol-based highly conductive polymer for conformal nanocoatings on hydrophobic surfaces toward a highly sensitive and stable pressure sensor. *NPG Asia Mater.* **12**, 65 (2020).
- 36. Y.-T. Tseng, Y.-C. Lin, C.-C. Shih, H.-C. Hsieh, W.-Y. Lee, Y.-C. Chiu, W.-C. Chen, Morphology and properties of PEDOT:PSS/soft polymer blends through hydrogen bonding interaction and their pressure sensor application. *J. Mater. Chem. C* **8**, 6013-6024 (2020).
- 37. L. Sun, S. Jiang, Y. Xiao, W. Zhang, Realization of flexible pressure sensor based on conductive polymer composite *via* using electrical impedance tomography. *Smart Mater. Struct.* **29**, 055004 (2020).
- 38. Y. Li, C. Jiang, W. Han, Extending the pressure sensing range of porous polypyrrole with multiscale microstructures. *Nanoscale* **12**, 2081-2088 (2020).
- 39. J.-C. Wang, R. S. Karmakar, Y.-J. Lu, S.-H. Chan, M.-C. Wu, K.-J. Lin, C.-K. Chen, K.-C. Wei, Y.-H. Hsu, Miniaturized flexible piezoresistive pressure sensors: poly(3,4-ethylenedioxythiophene):poly(styrenesulfonate) copolymers blended with graphene oxide for biomedical applications. *ACS Appl. Mater. Interfaces* 11, 34305-34315 (2019).
- 40. Z. Wang, Y. Si, C. Zhao, D. Yu, W. Wang, G. Sun, Flexible and washable poly(ionic liquid) nanofibrous membrane with moisture proof pressure sensing for real-life wearable electronics. *ACS Appl. Mater. Interfaces* **11**, 27200-27209 (2019).

- 41. Y.-J. Tsai, C.-M. Wang, T.-S. Chang, S. Sutradhar, C.-W. Chang, C.-Y. Chen, C.-H. Hsieh, W.-S. Liao Multilayered Ag NP-PEDOT-paper composite device for human-machine interfacing. *ACS Appl. Mater. Interfaces* 11, 10380-10388 (2019).
- 42. J. Oh, J.-H. Kim, K. T. Park, K. Jo, J.-C. Lee, H. Kim, J. G. Son, Coaxial struts and microfractured structures of compressible thermoelectric foams for self-powered pressure sensors. *Nanoscale* **10**, 18370-18377 (2018).
- 43. O. Y. Kweon, S. J. Lee, J. H. Oh, Wearable high-performance pressure sensors based on three-dimensional electrospun conductive nanofibers. *NPG Asia Mater.* **10**, 541-551 (2018).
- 44. K. Qi, J. He, H. Wang, Y. Zhou, X. You, N. Nan, W. Shao, L. Wang, B. Ding, S. Cui, A highly stretchable nanofiber-based electronic skin with pressure-, strain-, and flexion sensitive properties for health and motion. *ACS Appl. Mater. Interfaces* **9**, 42951-42960 (2017).
- 45. W. W. Nichols, Clinical measurement of arterial stiffness obtained from noninvasive pressure waveforms. *Am. J. Hypertens.* **18**, 3S–10S (2005).
- 46. J. Park, J. Kim, J. Hong, H. Lee, Y. Lee, S. Cho, S.-W. Kim, J J. Kim, S. Y. Kim, H. Ko, Tailoring force sensitivity and selectivity by microstructure engineering of multidirectional electronic skins. *NPG Asia Mater.* **10**, 163-176 (2018).
- 47. C. Dagdeviren, Y. Su, P. Joe, R. Yona, Y. Liu, Y.-S. Kim, Y.A. Huang, A. R. Damadoran, J. Xia, L. W. Martin, Y. Huang. J. A. Rogers, Conformable amplified lead zirconate titanate sensors with enhanced piezoelectric response for cutaneous pressure monitoring. *Nat. Commun.* 5, 4496 (2014).
- 48. S. G. Im, K. H. Gleason, Systematic control of the electrical conductivity of Poly(3,4-ethylenedioxythiophene) via oxidative chemical vapor deposition. *Macromolecuels* **40**, 6552-6556 (2007).
- 49. S. Lee, D. C. Paine, K. K. Gleason, Heavily doped poly(3,4-ethylenedioxythiophene) thin films with high carrier mobility deposited using oxidative CVD: Conductivity stability and carrier transport, *Adv. Funct. Mater.* **24**, 7187-7196 (2014).
- 50. S. Liu, T. Hua, X. Luo, N. Y. Lam, X.-M. Tao, L. Li, A novel approach to improving the quality of chitosan blended yarns using static theory. *Text. Res. J.* **85**, 1022-1034 (2015).
- 51. C. Pang, G.-Y. Lee, T. Kim, S. M. Kim, H. N. Kim, S.-H. Ahn, K.-Y. Suh, A flexible and highly sensitive strain-gauge sensor using reversible interlocking of nanofibers, *Nat. Mater.* 11, 795-801 (2012).
- 52. F. Q. Al-Khalidi, R. Saatchi, D. Burke, H. Elphick, S. Tan, Respiration rate monitoring methods: A review, *Pediatr. Pulmonol.* **46**, 523-529 (2011).
- 53. S. Fleming, T. DPhil, R. Stevens, C. Heneghan, A. Plüddemann, I. Maconochie, L. Tarassenko, D. Mant, Normal ranges of heart rate and respiratory rate in children from birth to 18 years of age: A systematic review of observational studies. *Lancet.* **377**, 1011-1018 (2011).
- 54. S. D. Kelly, M. A. E. Ramsay, Respiratory Rate Monitoring: Characterizing Performance for Emerging Technologies. *Anesth. Analg.* **119**, 1246-1248 (2014).
- 55. A. Rodríguez-Molinero, L. Narvaiza, J. Ruiz, C. Gálvez-Barrón, Normal Respiratory Rate and Peripheral Blood Oxygen Saturation in the Elderly Population. *J. Am. Geriatr. Soc.* **61**, 2238-2240 (2013).

- 56. P. Kovacik, G. Hierro, W. Livernois, K. K. Gleason, Scale-up of oCVD: Large-area conductive polymer thin films for next-generation electronics. *Mater. Horiz.* **2**, 221-227 (2015).
- 57. L. K. Allison, T. L. Andrew, A Wearable All-Fabric Thermoelectric Generator. *Adv. Mater. Technol.*, **4**, 1800615 (2019).

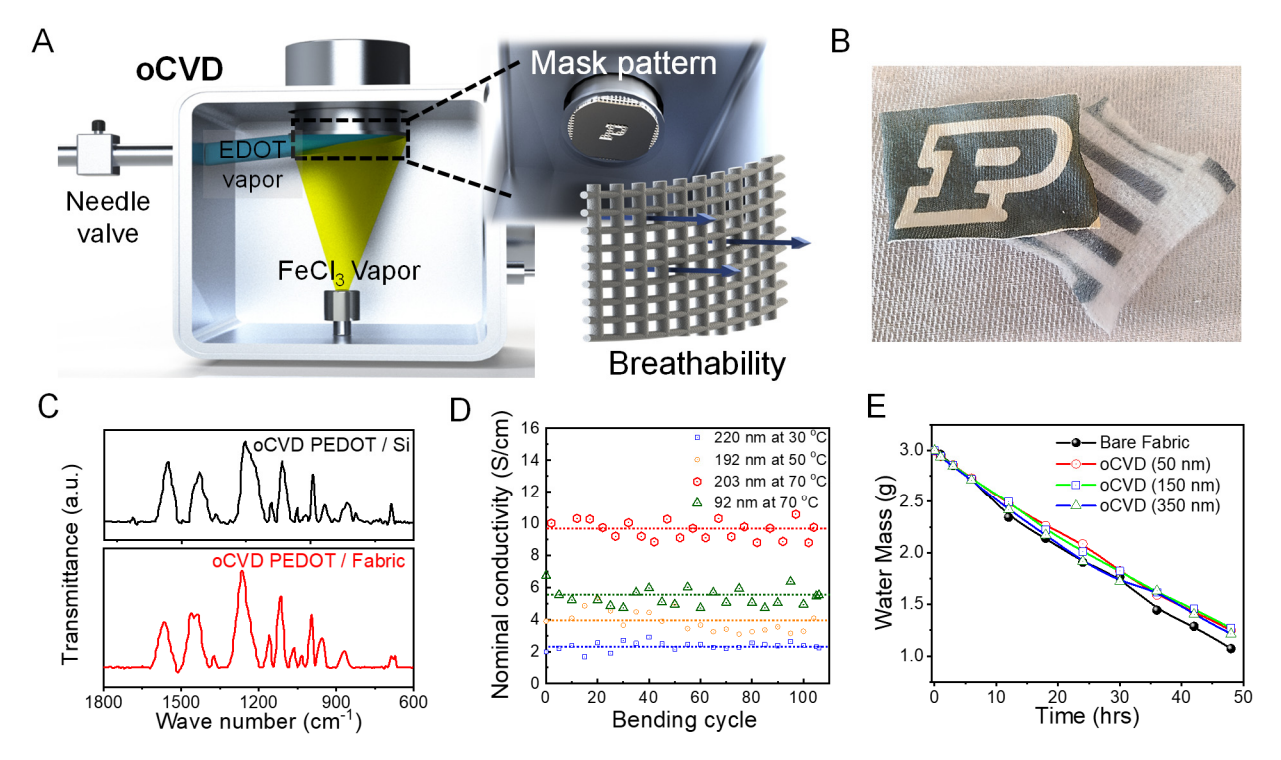


Fig. 1. Characterization of oCVD PEDOT. (A) Schematic of oCVD process. (B) Photo-image of patterned oCVD PEDOT on fabrics: Polyester (Left) and Gauze (Right). (C) FTIR spectra of oCVD PEDOT deposited on silicon and polyester substrates. (D) Conductivity and bendability of oCVD PEDOT deposited on polyester with different thickness and deposition temperatures. (E) Breathability test of bare and oCVD PEDOT coated fabric. Photo Credit: Hyeonghun Kim, Purdue University

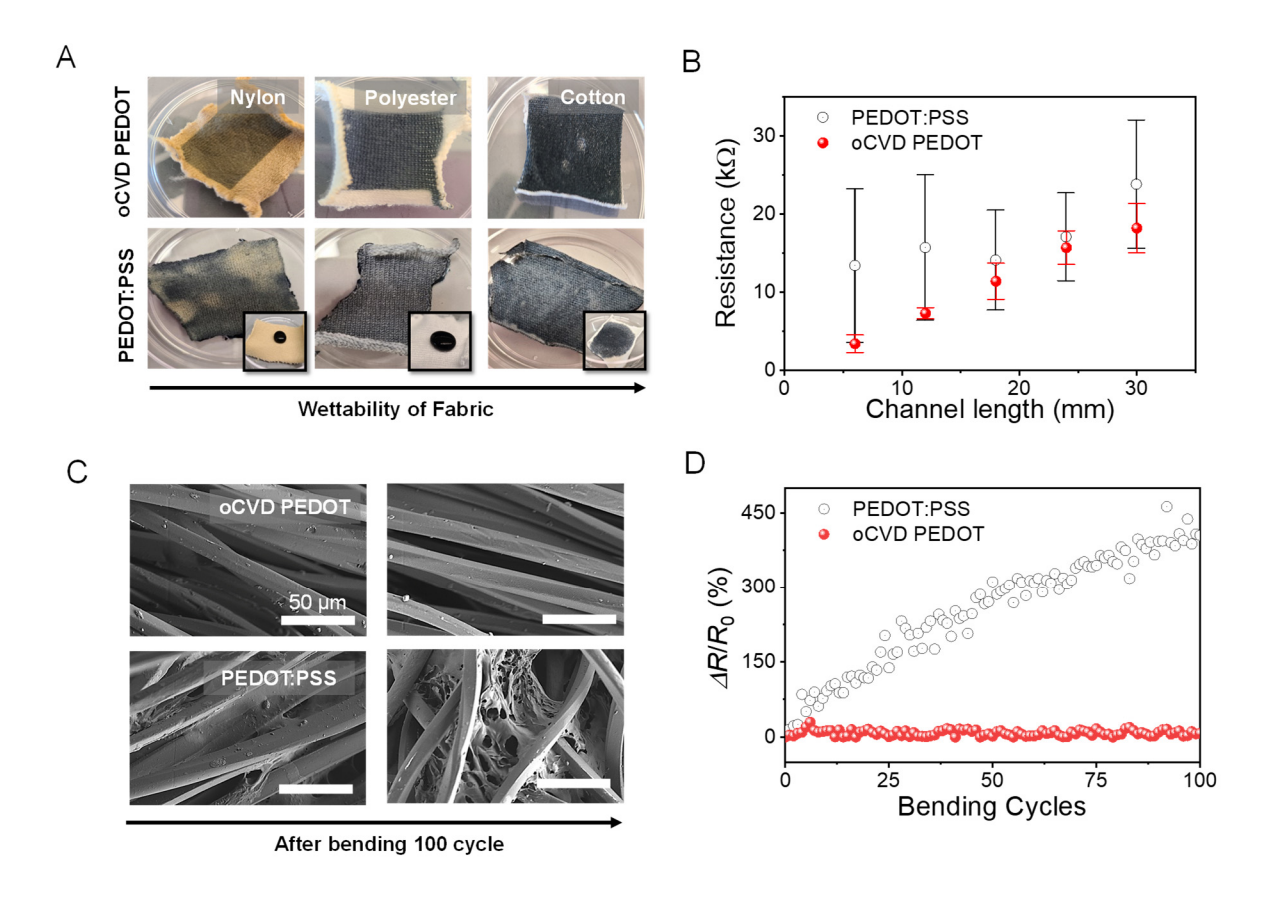


Fig. 2. Comparison between oCVD PEDOT and PEDOT:PSS. (A) Photo-images of fabrics (nylon, polyester, and cotton) coated by oCVD PEDOT and PEDOT:PSS. The insets demonstrate a droplet of PEDOT:PSS solution on each fabric, representing the fabric's hydrophobicity. (B) Uniformity tests: fabricating multiple electrode pairs on PEDOT coated polyesters using silver paste with a channel width of 6 mm and different channel lengths from 6 to 30 mm. (C) SEM images of oCVD PEDOT and PEDOT:PSS on polyester before and after bending 100 cycles. (D) Resistance change during the bending tests. Photo Credit: Hyeonghun Kim, Purdue University

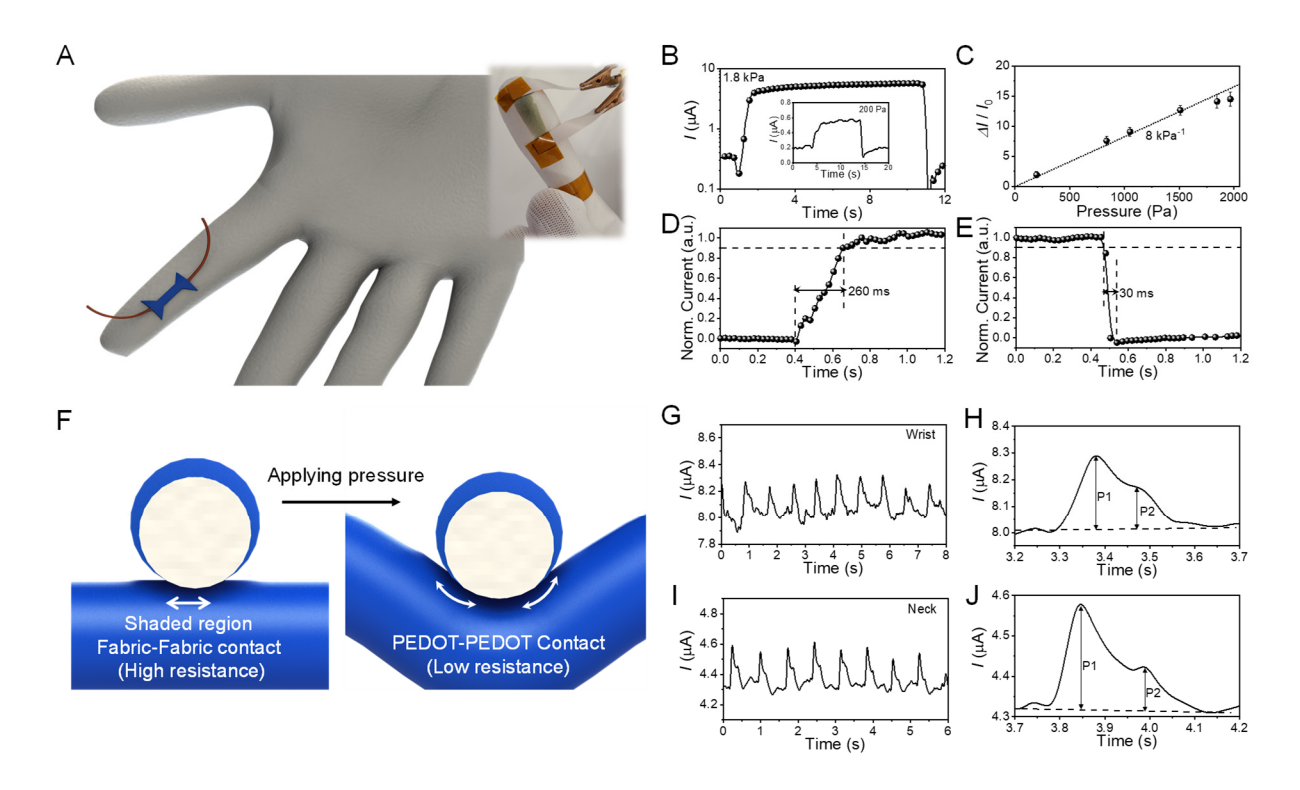


Fig. 3. oCVD PEDOT on the glove for blood pressure sensor. (A) A schematic and photo-image of oCVD PEDOT sensor fabricated on a polyester glove. (B) Transient current curve, recorded at 0.1 V under applying a pressure of 1.8 kPa. The inset demonstrates current change occurring under a pressure of 200 Pa. (C) Current change occurring under different pressure. The slope represents the sensitivity of the sensor. (D) Response and (E) recovery times, measured applying 1.8 kPa. (F) A schematic showing a working mechanism of the oCVD PEDOT pressure sensor. (G to J) Blood pressure measurements. (G) The radial artery blood pressure recording by placing the sensor on the wrist and (H) an extended image of it showing a single pulse; (I) the carotid artery blood pressure recording by placing the sensor on the neck and (J) an extended image of it showing a single pulse. Photo Credit: Hyeonghun Kim, Purdue University

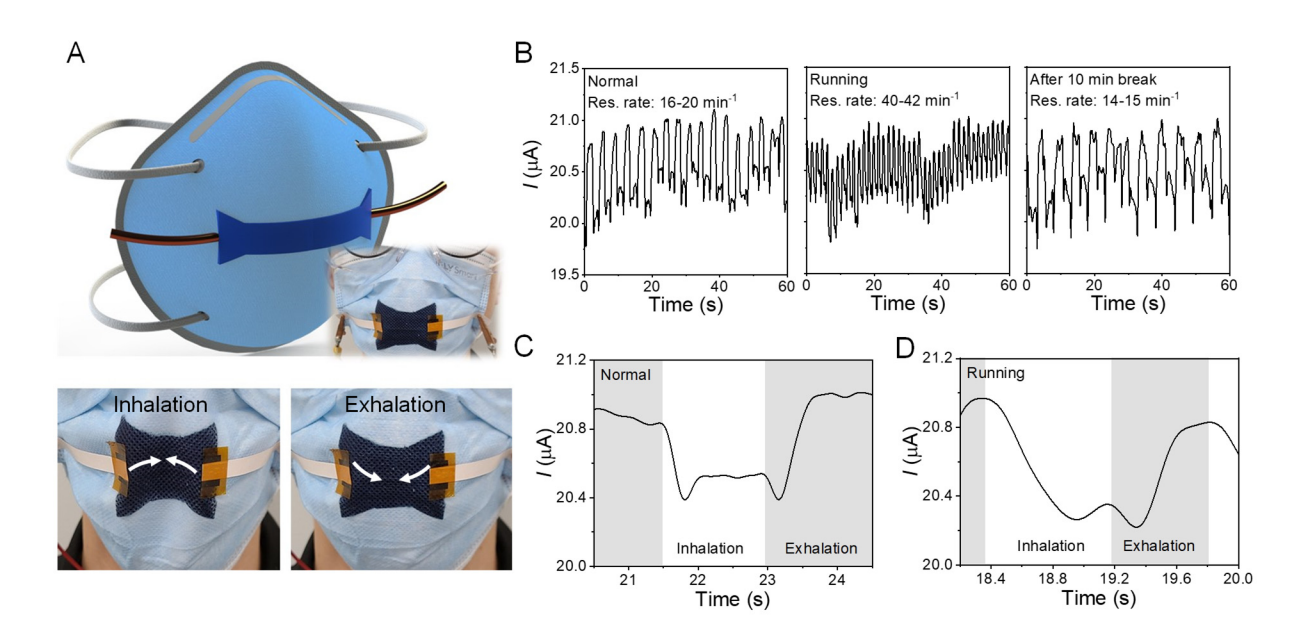


Fig. 4 oCVD PEDOT on the mask for respiratory rate sensor. (**A**) Schematic and photo images of oCVD PEDOT sensor fabricated on a disposable mask. The top images demonstrate a schematic of the mask sensor and an actual sensor image; the bottom photo images represent the instant deformation of the mask during inhalation and exhalation. (**B**) Breath patterns measured at an initial state (left), after 10 min exercise (middle), and further 10 min break (right). A single respiratory pattern, measured at (**C**) the normal and (**D**) as soon as after the exercise. Photo Credit: Michael Clevenger and Hyeonghun Kim, Purdue University